Arab J. Nucl. Sci. Appl., Vol. 52, 4, 145-158 (2019)

Arab Journal of Nuclear Sciences and Applications

ISSN 1110-0451 ***Web site: ajnsa.journals.ekb.eg*** **(ESNSA)**

Structure, Optical and Thermal Properties of Gamma Irradiated PVA/$Cd_{0.9}Mn_{0.1}S$ Nanocomposite Films

***A. AbouElfadl*[1,2]**

[1] *Physics Department, Faculty of Science, Taibah University, Al-Madina al Munawarah, Saudi Arabia*

[2] *Physics Department, Faculty of Science, Fayoum University, Fayoum, Egypt*

Received 8th Feb. 2019
Accepted 6th Mar. 2019

Nanocomposite films of PVA and $Cd_{0.9}Mn_{0.1}S$ prepared viasolution casting method were exposed todifferent doses of gamma radiation.Several techniques have been applied to emphasize the effects of gamma ray on the properties of the nanocomposite sample. Induced structural changes were investigated by X-ray diffraction (XRD) and Fourier transform infrared (FTIR), whereas UV-vis spectroscopy and differential thermal analysis (DTA) were used to study irradiation effects on the optical and thermal properties of samples. XRD and FTIR revealed that the structure of samples is strongly affected byirradiation and the crosslinking is the dominant process.The estimated values of the optical energy gap, E_g, Urbach energy, E_U, and different optical parameters exhibited dose dependence. The direct optical energy gap of thepristine sample is about 5.47 eV, and decreases with irradiation to a value of 2.9eV for 120 kGy irradiatedsample. The observed increase in refractive index and Urbach energy with irradiation confirmed the reduction in the ordered structure of the samples because of crosslinking. The color difference between the irradiated samples and the pristine one,ΔE, increases from 1.6 to 73.8with increasing the gamma dose. DTA data indicate that increasing the dose decreases the melting point, which can be attributed to defects generation by irradiation.

Keywords: *Nanocomposite, XRD, UV-vis spectroscopy, FTIR, DTA*

Introduction

Nanosized materials have been constructed with optical and electronic properties differing from those of their bulk phase [1]. Polymer matrix nanocomposites are becoming an essential part of today's materials because of several advantages such as low weight, simple fabrication methods, low cost, high fatigue strength, and good corrosion resistance. Nanoparticles incorporation into the polymer matrix considerably alters its physical properties such as the electrical, structural, thermal and optical properties [2-3].PVA is a semi-crystalline polymer having a high dielectric strength, good thermo-stability, high mechanical strength, chemical resistance, excellent film forming properties and optical transparency [4-6]. The existence of the hydroxyl group, (–OH), gives PVA special properties due to the strong –OH interaction between intra and inter-molecular polymer chains [7]. The two-dimensional hydrogen bonding of PVA enhances the formation of polymer complexes after reacting with other functional polymers and compounds [8]. In addition, PVA is a biocompatible, fully biodegradable and non-toxic water-soluble polymer [9]. It has gained increasing attention for biomedical applications [10].

PVA-based nanocomposites combine the properties of both additives and polymers. Adding specified nanoparticles into the PVA matrix could modify its properties to be suitable for a particular application. These nanocomposites have several applications in medical and engineering technology because of their electron transport, mechanical and optical properties [11-12].

Corresponding author: azzaaboelfadl@yahoo.com

DOI: 10.21608/ajnsa.2019.8081.1177

© Scientific Information, Documentation and Publishing Office (SIDPO)-EAEA

Semiconductor nanoparticles have acquired increasing concern due to their extensive applications in optoelectronics, photovoltaics, lasing, bio-labeling, etc. [13-17]. The quantum confinement effect gives the semiconductor nanoparticles their unique size-dependent optical properties. The confinement effect is detected for CdS particles of sizes equal to or less than 5 nm [18]. CdS shows interesting optical properties [19-20]. The influences of many additives on the photoluminescence property of CdS nanoparticles have been studied [21]. CdS/PVA nanocomposite have gained extensive consideration because of the wide direct band gap of CdSas well as good elastic, mechanical and acoustic properties of PVA.

High-energy radiation as gamma rays is utilized to produce physical and chemical changes, e.g., density, molecular weight distribution, crystallinity and solubility, either by the excitation of polymer molecules or formation of freely moving ions. Many properties of polymers are molecular weight dependent. The main phenomena associated with radiation–polymer interaction are chain crosslinking, causing an increase in the molecular weight, chain scission, causing decrease in molecular weight, and emission of atoms, molecules and molecular fragments [22].

The present study aims at investigating the induced changes of PVA/$Cd_{0.9}Mn_{0.1}S$ nanocomposites to gamma irradiation. XRD and FTIR techniques are employed to probe the structural changes with gamma doses. In addition, optical investigation yields valuable information about energy band gap, refractive index and color intensity. DTA technique is utilized to understand the influence of irradiation on the thermal properties of the nanocomposite samples.

Experimental

Preparation of PVA/$Cd_{0.9}Mn_{0.1}S$ nanocomposite films

Nanoparticles of $Cd_{0.9}Mn_{0.1}S$ were synthesized following the procedure described elsewhere [23]. In order to prepare PVA/$Cd_{0.9}Mn_{0.1}S$ nanocomposite films, solution casting technique was used. An aqueous PVA solution was obtained by dissolving 2 g of PVA powder (supplied by Sigma-Aldrich GMBH) in 100 ml double distillated water under continuous stirring at 90^{o}C for 3 h. The required mass of $Cd_{0.9}Mn_{0.1}S$ nanoparticles (weight percentage 5%) was carefully mixed with the PVA solution under strong stirring to avoid any agglomeration. Final homogeneous solution was poured into Petri dishes and dried at 40^{o}C forming nanocomposite films. The obtained films of 0.1 mm thickness were cut into square pieces to be suitable for measurements.

Irradiation facilities

The films were irradiated by different gamma doses in the range 10-120 kGy from ^{60}Co source at room temperature at a dose rate of 2.4 Gy/min and region energies of 1.173 and 1.332 MeV at Atomic Energy Authority (AEA), Cairo, Egypt.

Materials characterization

X-ray diffraction (XRD) analysis was performed using a Philips diffractometer type PW 1373 goniometer with Cu K_{α} radiation (λ = 0.154 nm). XRD patterns were recorded in the 2θ range (10–80°) with scanning rate of 2^{o}/min and a step of 0.02°.

Fourier transform infrared, FTIR, spectra were analyzed. A Shimadzu, Model 8201 PC spectrophotometer in the range of 400–4000 cm^{-1}wavenumber is used. The measurement accuracy is ±4 cm^{-1}.

The UV/Vis spectra of all samples were acquired by Tomos UV-1800 spectrophotometer. The spectral distribution of transmittance T (λ) was recorded in the wavelength range of 190-1000 nm. The sample color was described by CIE tri stimulus values and the CIELAB color space approach that was previously reported[24]. A uniform color space facilitates the formation of a reliable color difference ruler between two samples. This is important in the radiation dosimetry field. Mathematical equations were previously described in detail [24].

Thermal analysis of samples was performed using a Shimadzu DTA-50, Differential Thermal Analyzer, with platinum cells. DTA measurements were achieved with α-Al2O3 reference material under nitrogen atmosphere (30 ml/ min) at a heating rate of 20 $^{\circ}$C/min. using the temperature ranging from 25 to 250 ^{o}C

Results and Discussion

The Rietveld refinement fitting, lattice parameters, phase analysis and element distribution of Cd, Mn and S of the prepared $Cd_{0.9}Mn_{0.1}S$ nanoparticle were reported before by Mohamed, et al. [23]. XRD patterns of PVA/$Cd_{0.9}Mn_{0.1}S$ nanocomposite

samples are depicted in Figure (1). As clearly shown, all XRD patterns reveal the semi-crystalline nature of the investigated nanocomposites samples. A relatively sharp diffraction peak was observed at about $2\theta = 19.5^{o}$ corresponding to the diffraction from the (101) plane and d spacing of 4.51Å [25-27]. Additionally, a small peak was observed at about $2\theta = 40.7^{o}$ indicating the semi-crystalline structure of PVA arising from intra- and intermolecular hydrogen bond of chains[28].Figure (2) shows the dependence of the integral intensity of the main diffraction peak at 20^{o} on the gamma dose. As shown, the integral intensity decreases with increasing the dose implying a reduction in the main chains order of the polymeric molecules of the nanocomposites upon irradiation. The decrease in X-ray intensity might be due to the crosslinking that could disrupt the hydrogen bonding of the PVA chains. $Cd_{0.9}Mn_{0.1}S$ nanoparticles could be implanted in the PVA matrix by forming new bonds between them and PVA chains that leads to a drop in the degree of crystallinity.

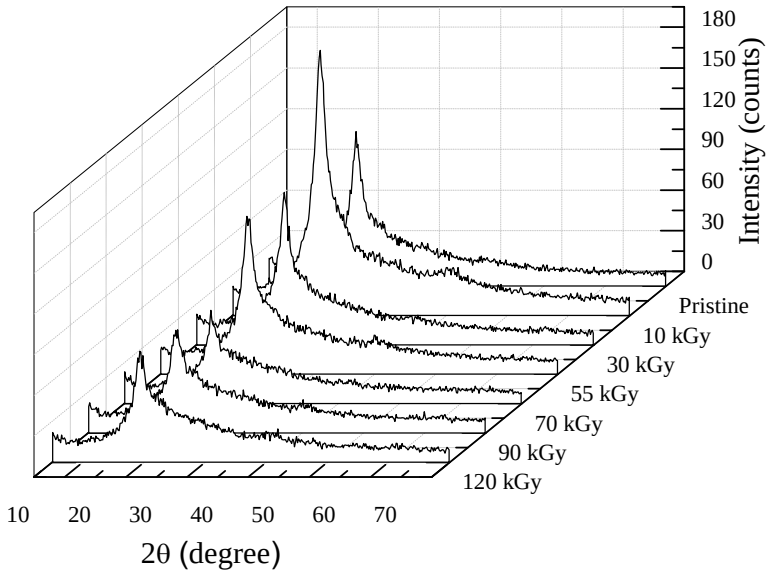

Figure (1): XRD patterns of the pristine and irradiated PVA/$Cd_{0.9}Mn_{0.1}S$ nanocomposite films

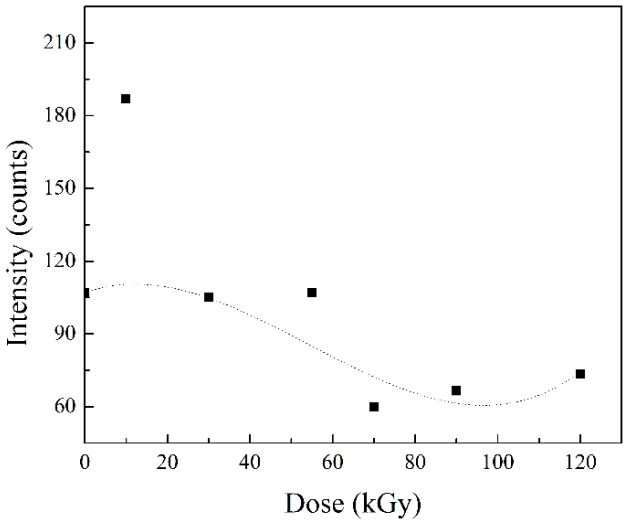

Figure (2): The integral intensity I of the main diffraction peak at 20^{o}versus the gamma dose

FT-IR absorption spectra of the pristine and irradiated PVA/ $Cd_{0.9}Mn_{0.1}S$ nanocomposite samples are presented in Figure (3). All spectra exhibit the characteristic bands of PVA at the wavenumbers 3271, 2919, 1712, 1653, 1080, 918 cm^{-1}. The observed vibrations at 3271 cm^{-1} and 1653 cm^{-1} are attributed to the O-H stretching vibrations for intermolecular and intramolecular hydrogen bonds of PVA [29-31]. The CH_2 asymmetric stretching vibration is observed at 2919 cm^{-1}. Bands at 1712 and 1080 cm^{-1} are assigned to the symmetric C=O stretching and C-O stretching vibration, respectively. The band corresponding to C=C vibration occurs at 1653 cm^{-1}. Lastly, out of-phase C-C-O stretching is observed at 1080 cm^{-1} [30].

The induced changes have been estimated from the relative increase or decrease in the height of the peak associated to the functional groups present in the nanocomposite. Figure (3) shows the typical absorbance peaks which are summarized in Table (1). It is found that C-C absorbance band almost decreases nearby the 55 kGy- gamma dose, followed by an increase with dose up to 120 kGy indicating the predominance of the crosslinking process. Oxygen atoms of OH groups of PVA have lone pair electrons consequently regarded as good legends [32]. Concluding, coordination reactions occurred for hydroxyl group of PVA withCd^{2+} ions in the $Cd_{0.9}Mn_{0.1}S$ nanoparticles resulting in a coordination bond. A non-monotonic trend is observed for the intensity of C-H. Obviously, the intensity of the C-O bond, the carbonyl group C=O and the ethylene C=C bond exhibit almost a similar trend to that of C-C bond. The variation of the intensity of hydroxyl group, OH, confirms that the crosslinking is the dominant process.

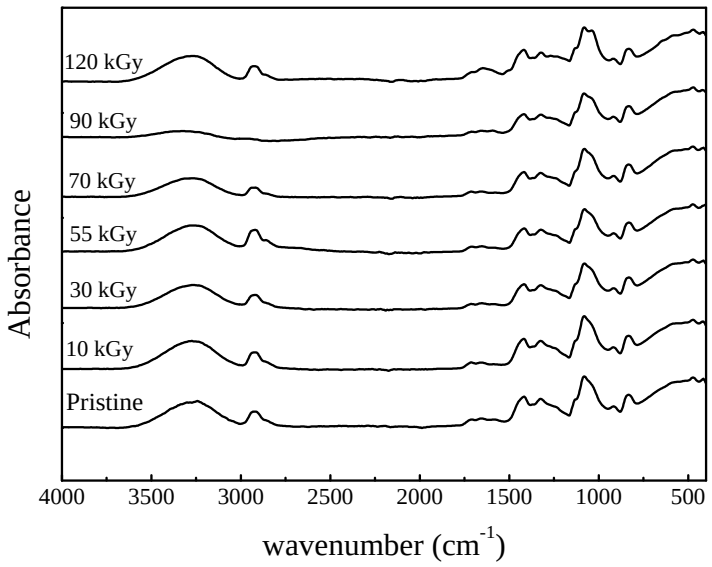

Figure (3): FTIR absorption spectra of the PVA/ $Cd_{0.9}Mn_{0.1}S$ nanocomposite films

Table (1): Absorbance of characteristic vibrations of PVA/ $Cd_{0.9}Mn_{0.1}S$ samples as a function of doses

Gamma dose (kGy)	Absorbance (a.u.)					
	C-C (918 cm^{-1})	C-H (2919 cm^{-1})	C-O (1080 cm^{-1})	C=O (1712 cm^{-1})	C=C (1653 cm^{-1})	OH (3271 cm^{-1})
0	0.206	0.157	0.492	0.0813	0.0913	0.243
10	0.205	0.157	0.502	0.0608	0.0593	0.265
30	0.189	0.126	0.425	0.0408	0.0471	0.22
55	0.187	0.218	0.416	0.0596	0.0626	0.261
70	0.201	0.0891	0.458	0.0507	0.0513	0.177
90	0.188	-	0.41	0.0461	0.0546	0.0527
120	0.221	0.15	0.519	0.0935	0.132	0.247

Spectral measurements have been performed to characterize PVA/ $Cd_{0.9}Mn_{0.1}S$ nanocomposite films. The UV–visible absorption spectra of nanocomposite films are presented in Figure (4). The absorbance variation with gamma doses suggests that the levels of the energy band were changed by the radiation and the Rayleigh scattering from the implanted $Cd_{0.9}Mn_{0.1}S$ nanoparticles [33,34].As shown, the spectrum of pristine sample revealed an absorption edge at about 230 nm. Obviously, the absorption edge shows a red shift upon irradiation.

The optical band gap and the electronic transitions mode that governs the optoelectronics performance of matters can be determined from the analysis of the absorption spectrum. The optical energy gap (E_g) of the nanocomposite films was computed from Tauc's relation [35]:

$$\alpha h\nu = B\left(h\nu - E_g \right)^m \quad (1)$$

Where, hν is the incident photon energy ($h\nu = 1240/\lambda$), α is the absorption coefficient, B is a constant and m is the power factor of the transition mode, that is dependent on the material nature. Power factor, m, is assumed to be 1/2 (allowed direct), 2 (allowed indirect), 3/2 (forbidden direct), and 3 (forbidden indirect) transitions. The absorption coefficient was computed using the following equation [36]:

$$\alpha = 2.303 \frac{A}{d} \quad (2)$$

Where d is the sample thickness and A is the absorbance. Direct energy gaps of the nanocomposite samples were evaluated by plotting $(\alpha h\nu)^2$vs. hν and extrapolating the linear part of $(\alpha h\nu)^2$ to zero on the x-axis. The dose-dependent direct energy gap is presented in Figure (5). As seen, the direct energy gap E_g of pristine sample of 5.47 eV was reduced to 2.9 eV with increasing gamma dose which could be attributed to crosslinking. New covalent bonds were formed between $Cd_{0.9}Mn_{0.1}S$ and PVA resulting in new different chains that hinder the mobility of molecules and decrease their activity, consequently reduce the optical band gap[37]. The variation of optical band gap infers that gamma irradiation modifies the electronic structure of nanocomposite samples.

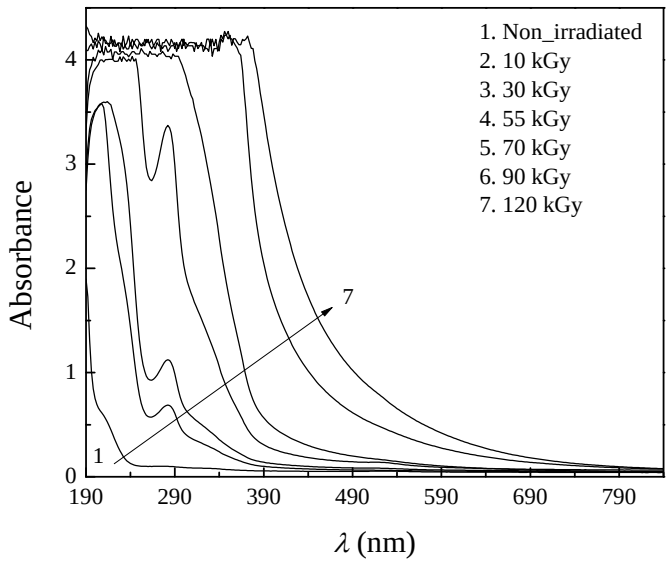

Figure (4): The UV–Vis absorption spectra of the PVA/$Cd_{0.9}Mn_{0.1}S$ nanocomposites films

Near the band edge, the absorption coefficient depends exponentially on the photon energy and obeys the empirical Urbach rule. This rule can be used for determining the band tail energy (E_U) of the localized states in the band gap associated with the structural defects and disorder within the polymer matrix. Urbach energy (E_U) can be determined using the following equation [38].

$$\alpha = \alpha_o exp\left(\frac{h\nu}{E_U}\right) \quad (3)$$

Where α_o is a constant that characterizes the materials. Urbach energy, E_U, could be estimated from the reciprocal of the straight-line slope of ln α versus hν plot. Figure (5) reveals that the values of E_U is dose dependent reaching a minimum at around the 30 kGy dose then increases with increasing dose up to 120 kGy. The increase of Eu values can be attributed to the effect of internal potential fluctuation associated with the increased structural disorder and defects upon irradiation, cf., Figure (1).

Using the absorbance (A) and transmission (T) spectra, the reflectance of PVA/$Cd_{0.9}Mn_{0.1}S$ nanocomposite samples was determined as follows [39]:

$$R = 1 - \sqrt{T * \exp(A)} \quad (4)$$

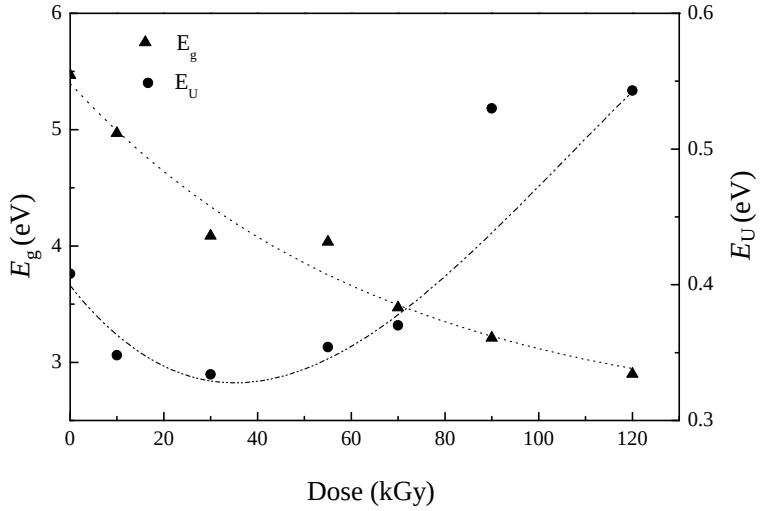

Figure (5): Dose dependence of Urbach's energy (E_U) and the direct energy gap (E_g) for PVA/$Cd_{0.9}Mn_{0.1}S$ nanocomposites films

Refractive index, n, is extremely important for optoelectronic and electronic applications. The refractive index, n, of samples is estimated from the reflectance (R) and extinction coefficient, k, (where $k = \alpha\lambda/4\pi$) using Fresnel relation [40]:

$$n = \left(\frac{1+R}{1-R}\right) + \sqrt{\frac{4R}{(1-R)^2} - k^2} \quad (5)$$

The calculated refractive index, n, is shown in Figure (6)as a function irradiation dose. The observed increase in the refractive index n with increasing the dose up to 120 kGy may be attributed to the crosslinking induced by gamma irradiation. The degradation and crosslinking processes may occur simultaneously until one of them dominates. The material properties depend strongly on its internal structure, including packing density and molecular weight distribution. The increase in the value of n of samples with increasing dose may be interpreted in terms of the formation of intermolecular crosslinking thereby the density increases, thus diminishing the anisotropic character of the nanocomposite samples. Additionally, the chain scission and crosslinking could vary the orientation of chains, and thusalter the refractive index [41].

Figure (7) shows the transmission spectra in the visible wavelength range 360-780 nm of PVA/ $Cd_{0.9}Mn_{0.1}S$ nanocomposite samples. The chromaticity coordinates (x, y, z), tristimulus values (X, Y, Z) and the uniform color space (L*, a* and b*) were computed by applying the transmittance values in the reported mathematical equations [24]. Tristimulus values of samples are

presented in Figure (8)as a function of gamma dose. Similar trend is observed for X, Y and Z in which they decreased on increasing the dose up to 120 k Gy. Dose dependence of chromaticity coordinates is shown in Figure (9). It is obvious that both x and y chromaticity coordinates increase with increasing dose, whereas chromaticity coordinate z exhibit an opposite trend. Color intercepts are presented as a function of gamma dose in Figure (10). A perfect white and a perfect black would have L* value of 100 and 0, respectively. Coordinate a* associates with red (+a*) and green (-a*) while the CIELAB coordinate b* associates with yellow (+b*) and blue (-b*) [24]. Figure 10 reveals that red (+a*) and yellow (+b*) components increase with doses while the lightness value, L*, shows a reduction with increasing gamma doses which is in a good agreement as supported by the observed behavior of the transmittance (T), cf. Figure (7). The observed behavior of the color intercepts indicates that nanocomposite samples tend to be more reddish yellow and darker with increasing dose up to 120 kGy.

In order to evaluate the coloration effects, the total color differences, ΔE, between the irradiated samples and the pristine one have been estimated and is displayed in Figure (10d) as a function of dose. A significant increase is observed in the color difference (ΔE) with the dose indicating that irradiation have pronounced effect on color parameters. Color changes can arise from the variation of microstructure resulting from a destruction of the chemical bonds and formation of energetic electrons and ions. Such energetic species can migrate in the polymer matrix producing more damage of molecules and may be trapped forming color centers [42, 43].

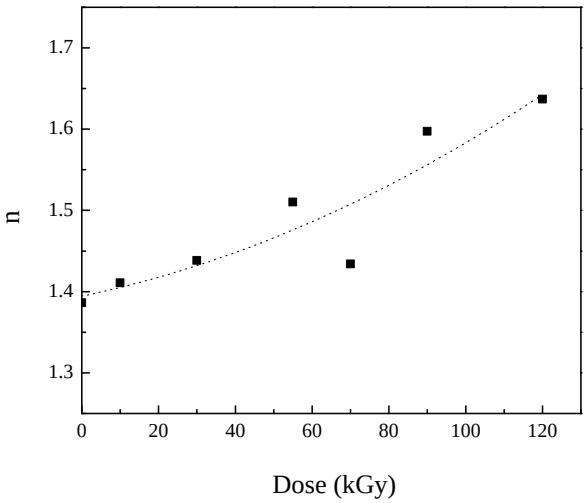

Figure (6): The refractive index, calculated at 800 nm, of PVA/$Cd_{0.9}Mn_{0.1}S$ as a function of gamma dose

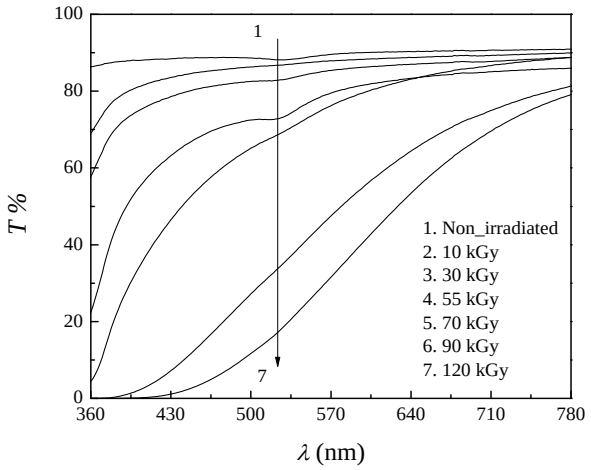

Figure (7): The transmission spectra in the visible wavelength of the pristine and irradiated PVA/ $Cd_{0.9}Mn_{0.1}S$ nanocomposite films

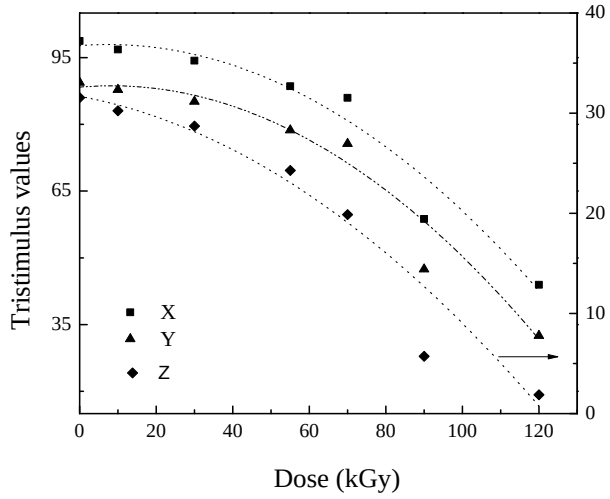

Figure (8): Dose dependence of the tristimulus values for PVA/$Cd_{0.9}Mn_{0.1}S$ nanocomposites films

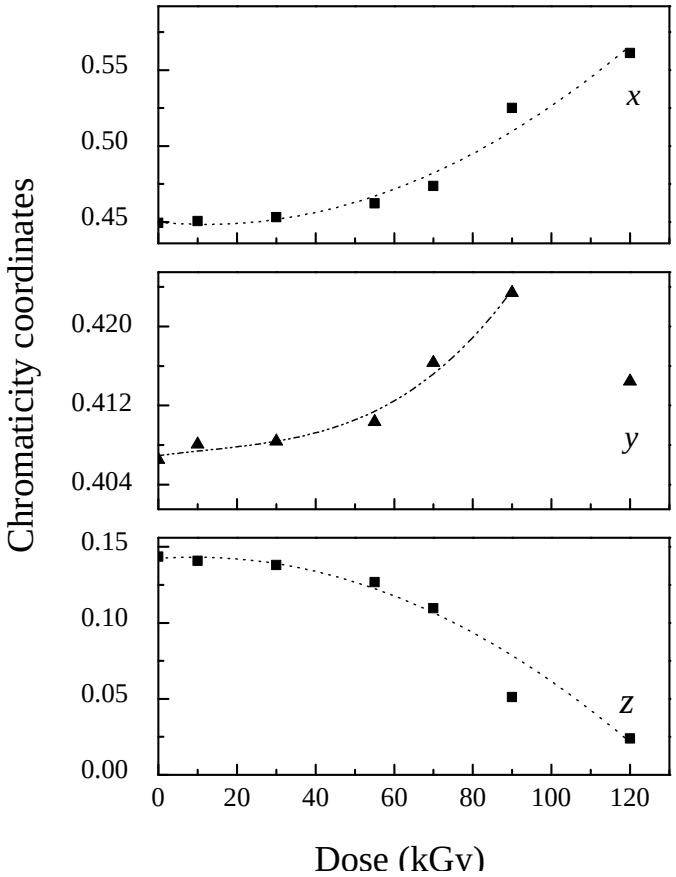

Figure(9):Dose dependence of the chromaticity coordinates for PVA/$Cd_{0.9}Mn_{0.1}S$ nanocomposites films

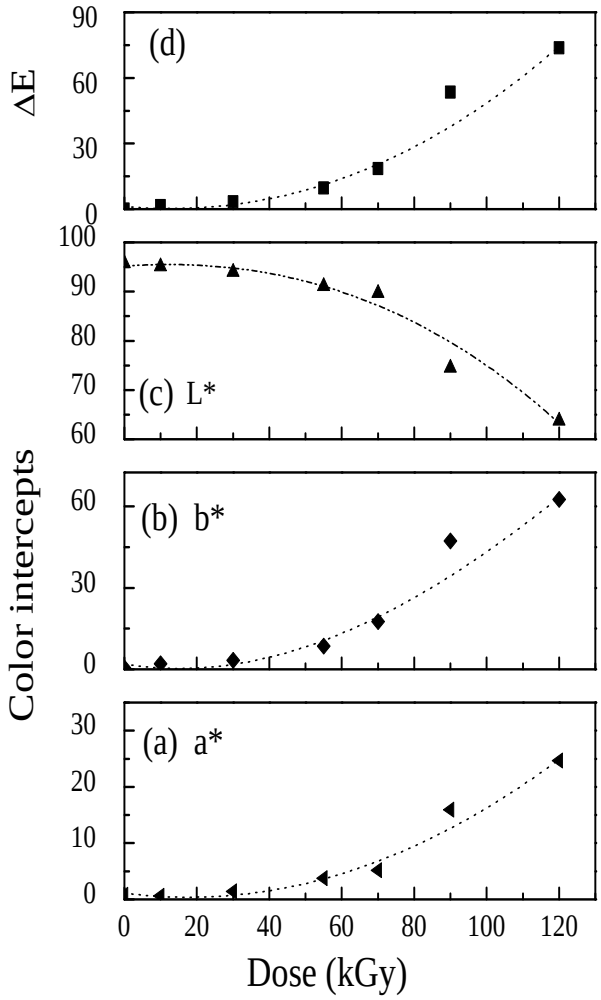

Figure(10):Dose dependence of the color intercepts and color intensity ΔE for PVA/$Cd_{0.9}Mn_{0.1}S$ nanocomposites films

DTA technique was applied to examine the thermal properties of PVA/ $Cd_{0.9}Mn_{0.1}S$ nanocomposites. The DTA heating curves up to 250^{o}C of pristine and irradiated samples are shown in Figure (11). Two endothermic peaks were distinguishable. The first peak at about 75^{o}C is assigned to glass transition, T_g, resulting from micro-Brownian motion of the PVA chain in the amorphous region. The second peak at 219^{o}C is due to melting transition, T_m. It is clear that the shape and position of the endothermic peaks are dose dependent. Clear inspection reveals that T_g is too weak and/or too broad to be detected for the non-irradiated, 30 and 55 kGy irradiated samples. Melting temperature was assessed at the position of the peak maximum and was represented as a function of dose in Figure (12). As shown, T_m decreases with increasing doses. Melting point is regarded as a sense of the crystalline domains of the polymer. Lowering T_m could be attributed to the creation of defects by gamma irradiation that splits the crystals, which depresses the melting temperature. Further, the reduction of the chain length shifts the values of T_m towards lower temperatures [44].

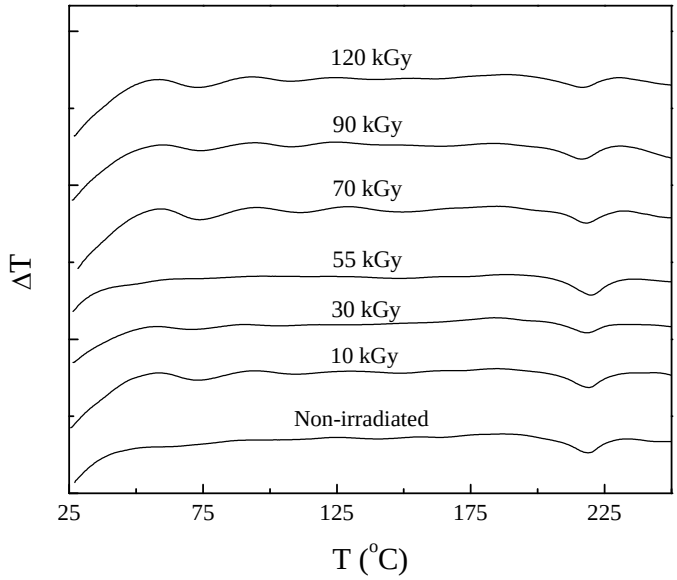

Figure (11): DTA thermograms for the pristine and irradiated PVA/$Cd_{0.9}Mn_{0.1}S$ nanocomposites

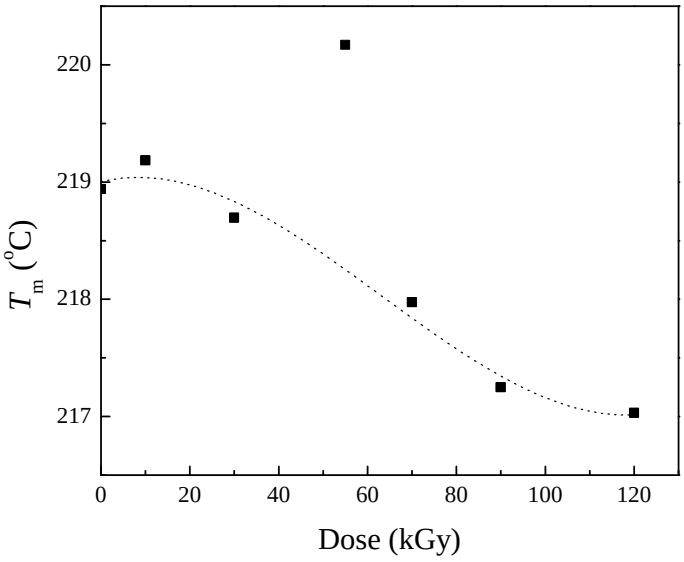

Figure (12): The melting temperatures, T_m, versus the gamma dose for PVA/$Cd_{0.9}Mn_{0.1}S$ nanocomposites

Conclusion

The solution casted PVA/$Cd_{0.9}Mn_{0.1}$Snanocomposite films were prepared and were irradiated with gamma doses in the range 10–120 kGy. The structure, optical and thermal properties of samples have been carefully investigated. XRD patterns showed a semi-crystalline structure with a relatively sharp peak at $2\theta = 19.5^{o}$. The reduction in the intensity of the crystalline peak with gamma irradiation indicates that the predominant process is crosslinking resulting in decreasing the degree of crystallinity. The UV-Vis absorption spectra were shifted to higher wavelengths upon gamma irradiation. Consequently, a significant decrease in the direct

optical band gap was observed. Furthermore, Urbach energy and refractive index were also influenced and increased with gamma irradiation. These results could be related to the increase in the structural disorder of the irradiated PVA/$Cd_{0.9}Mn_{0.1}$Snanocomposite due to the formation of crosslinks between OH of PVA and $Cd_{0.9}Mn_{0.1}$Snanoparticles and/or between PVA chains. FTIR results and lowering the melting temperature as revealed from DTA thermogram confirm that gamma irradiation doses up to 120 kGy leads to the predominance of the crosslinking. A considerable increase in the color differences between the irradiated samples and pristine one suggests that gamma irradiation creates color centers because of the variation of microstructure. This establishes the basis that can be applied in constructing a simple sensor for gamma irradiation.

References

1-Alivisatos, A.P. (1996) Semiconductor Clusters, Nanocrystals, and Quantum Dots, *Science*, 271, 933-937.

2-Mahendia, S., Tomar, A.K. and Kumar, S. (2011) Nano-Ag doping induced changes in optical and electrical behaviour of PVA films ,*Mater. Sci. Eng. B*, 176, 530-534.

3-Mahendia, S., Tomar, A.K. and Kumar, S. (2010)Electrical conductivity and dielectric spectroscopic studies of PVA–Ag nanocomposite films, *J. Alloys Compd*. 508, 406-411.

4-Abargues, R., Marqu_es-Hueso, J., Canet-Ferrer, J., Pedrueza, E., Vald_es, J. L., Jimenez E. and Martinez-Pastor J. (2008) High resolution electron beam patternable nanocomposite containing metal nanoparticles for plasmonics, *Nanotechnology* , 19, 355308-355311.

5-Abargues, R., Gradess, R., Canet-Ferrer, J., Abderrafi, K., Vald_es, J. L. and Martı´nez-Pastor J. (2009) Scalable heterogeneous synthesis of metallic nanoparticles and aggregates with polyvinyl alcohol, *New J. Chem.*, 33, 913-917.

6-Porel, S., Singh, S., Harsha, S.S., Rao, D.N. and Radhakrishnan T.P. (2005) Nanoparticle embedded polymer: In situ synthesis, free standing films with highly monodispersed silver nanoparticles and optical limiting, *Chem. Mater.*, 17, 9-12.

7-Yang, G., Wan, X., Liu, Y., Li, R., Su, Y. and Zeng, X.J. (2016) Tang, Luminescent poly(vinylalcohol)/ carbon quantum dots composites with tunable water-induced shape memory behavior in different pH and temperature environments, *ACS Appl. Mater. Interfaces*, 8, 34744–34754.

8-8. Bunyatova, U., Rzayev, Z., Koçum, İ., Şimşek, M. and Yürüksoy, M. (2016) Fabrication and Characterization of AgNPs Incorporated PVA/ODA-MMT and PVP/ODA-MMT Nanofiber Structures by Green Electrospinning Nanotechnology as Excellent Conducting and Bioengineering Nanomaterial, *ActaPhysicaPolonica A*, 129, 431-435.

9-El-Gamal, S., Ismail, A.M. and El-Mallawany, R. (2015) Dielectric and nano-scale free volume properties of polyaniline /polyvinyl alcohol nanocomposites, *J. Mater. Sci.: Mater. Electron*, 26, 7544–7553.

10-Cholakis, C. H., Zingg, W. and Seffon, M. V (1989) Effect of heparin–pva hydrogel on platelets in a chronic canine arterio-venous shunt, *J. Biomed Mater. Res*., 23, 417-441.

11-Bouropoulos, N., Psarras, G.C., Moustakas, N., Chrissanthopoulos, A. and Baskoutas, S. (2008)Optical and dielectric properties of ZnO-PVA nanocomposites, *Phys Status Solidi A*; 205,2033–2037.

12-Lee, J., Bhattacharyya, D., Easteal, A.J., Metson, J.B. (2008) Properties of nano-ZnO/poly(vinyl alcohol)/poly(ethylene oxide) composite thin films, *CurrApplPhys*, 8,42–47.

13-Murray, C.B., Norris, D.B. and Bawendi, M.G. (1993) Synthesis and characterization of nearly monodisperseCdE (E = sulfur, selenium, tellurium) semiconductor nanocrystallites, *J. Am. Chem. Soc.*, 115, 8706-8715.

14-Chestnoy, N., Harris, T.D. and Brus, L.E. (1986) Luminescence and photophysics of cadmium sulfide semiconductor clusters: the nature of the emitting electronic state,*J. Phys. Chem.*, 90, 3393-3399.

15-Spanhel, L., Haase, M., Weller, H. and Henglein, A. (1987) Photochemistry of colloidal semiconductors. 20. Surface modification and stability of strong luminescing CdS particles, *J. Am. Chem. Soc.*, 109, 5649-5655.

16-Wang, Y. and Herron, N. (1991) Nanometer-sized semiconductor clusters: materials synthesis, quantum size effects, and

photophysical properties, *J. Phys. Chem.*, 95, 525-532.

17-Alivisatos, A.P. (1996) Perspectives on the Physical Chemistry of Semiconductor Nanocrystals, *J. Phys. Chem.*, 100 (31), 13226-13239.

18-Wang, Y. and Herron, N. (1990) Quantum size effects on the exciton energy of CdS clusters, *Phys. Rev. B*, 42, 7253-7255.

19-Hillinski, E.F. and Lucas P.A. (1988) A picosecond bleaching study of quantum-confined cadmium sulfide microcrystallites in a polymer film, J. Chem. Phys., 89, 3435-3441.

20-Herron, N., Wang, Y. and Eckert, H. (1990) Synthesis and characterization of surface-capped, size-quantized cadmium sulfide clusters. Chemical control of cluster size, *J. Am. Chem. Soc.*, 112, 1322-1326.

21-Wu, X.C., Bittner, A.M. and Kern, K. (2005) Synthesis, Photoluminescence, and Adsorption of CdS/DendrimerNanocomposites, ,*J. Phys. Chem. B*, 109, 230-239.

22-Chapiro, A. (1998) Chemical modifications in irradiated polymers. *Nucl. Instrum. Methods B*, 32, 111–114.

23-Mohamed, M.B., Abdel-Kader, M.H., Alhazime, A.A. and Almarashi, J.Q. (2018) Effect of preparation methods and doping on the structural and tunable emissions of CdS, *J. Molec. Struct.*, 1155, 666-674.

24-Nassau, K. (1998) Color for Science, Art and Technology; Elsevier: New York.

25-El-Sayed, S., Abel-Baset, A., AbouElfadl, A. and Hassen, A. (2015) Effect of nanosilica on optical, electric modulus and AC conductivity of polyvinylalcohol/polyaniline films, *Physica B* 464, 17–27.

26-Sarma, S. and Datta, P. (2010) Characteristics of poly(vinyl alcohol)/lead sulphide quantum dot device., *Nanosci. Nanotechnol. Lett.*, 2, 261–265.

27-Shujahadeen, B.A.Z.I.Z. (2016) Modifying poly(vinyl alcohol) (PVA) from insulator to Small Band gap polymer: a novel approach for organic solar cells and optoelectronic devices. *J. Electron. Mater.*, 45, 736–745.

28-Chandrakala, H.N., Ramaraj, B., Shivakumaraiah, M. and Siddaramaiah, G. (2014) Optical properties and structural characteristics of zinc oxide-cerium oxide doped polyvinyl alcohol films, *J. Alloys Compd*. 586, 333–342.

29-Mansur, H.S., Sadahira, C.M., Souza, A.N., and Mansur, A.A.P. (2008) FTIR spectroscopy characterization of poly (vinyl alcohol) hydrogel with different hydrolysis degree and chemically crosslinked with glutaraldehyde, *Mater. Sci. Eng. C.*, 28 (4), 539–548.

30-Krimm, S., Liang, C.Y., Sutherland, G.B.B.M. (1956) Infrared spectra of high polymers. V.polyvinyl alcohol, *J. Polym. Sci*. XXII, 227–247.

31-Ali, Z.I. Ali, F.A. and Hosam, A.M. (2009) Effect of electron beam irradiation on the structural properties of PVA/V2O5 xerogel, *Spectrochim. Acta* A, 72 (4),868–875.

32-Ali, Z.I., Ebraheem, O., Saleh, H. H., Salam, F.H.A. and Sokary, R. (2015) In situ preparation of CdS/PVA nanocomposites using gamma radiation, *Polym. Eng. Sci*., 55, 2583-2590.

33-Rathore, B.S., Gaur, M.S. and Singh, K.S. (2012) Investigation of optical and thermally stimulated properties of SiO2 nanoparticles-filled polycarbonate, *J. Appl. Polym. Sci*., 126, 960-968.

34-Ilican, S., Caglar, Y., Caglar, M. and Yakuphanoglu, F. (2006) Electrical conductivity, optical and structural properties of Indium-doped ZnOnanofiber thin film deposited by spray pyrolysis method, *Phys. E*, 35, 131-138.

35-Tauc, J (1972) In: Abeles A (ed) The Optical properties of solid. North Holland, Amsterdam, p 277.

36-Muhammad, F.F. and Sulaiman, K. (2011) Utilizing a simple and reliable method to investigate the optical functions of small molecular organic films: Alq3 and Gaq3 as examples. Meas. *J. Int. Meas.Confed*. 44, 1468–1474.

37-Sayeda, E., Seif, E. and Nehad, M.(2014) Study the effect of gamma radiation on the optical energy gap of Poly(Vinyl Alcohol) based ferrotitanium alloy film: Its possible use in radiation dosimetry, *Open J. Polym. Chem*., 4, 21-30.

38-Urbach, F. (1953) The long-wavelength edge of photographic sensitivity and of the electronic absorption of solids, *Phys. Rev*. 92, 1324–1324.

39-Yahia, I. S., Farag, A. A. M., Cavas, M. and Yakuphanoglu, F. (2013) Effects of stabilizer ratio on the optical constants and optical

dispersion parameters of ZnOnano-fiber thin films, *Superlattices and Microstructures*, 53(1), 63–75, 201

40-Yakuphanoglu, F., Kandaz, M., Yarasir, M.N. and Senkal, F.B. (2007) Electrical transport and optical properties of an organic semiconductor based on phthalocyanine, *Physica B*, 393, 235-238.

41-Nouh, S. A., Abdel Salam, M. and Morsy, A. (2003) Electrical, optical and structural behaviour of fast neutron-irradiation-induced CR-39 SSNTD, *Radiation Measurements*, 37, 25-29.

42-Ludosik, D. and Macko, P. (1981) Vickers hardness number of neutron irradiated chalcogenide Ge-S glasses, *J. Non-Cryst. Solids*, 44, 397 (1981).

43-Abd-EI Kader, F.H., Said, G., Attia, G. and Abo-El Fadl A. M. (2006) Study of Structural and Optical Properties of Ethylene-Vinyl Acetate Copolymer Films Irradiated with γ-Rays, *Egypt. J. Phys.*, 37(2), 111-126.

44-Nouh. S. A. and Hegazy, T.M.(2006) Fast neutron irradiation effects on CN-85 solid state nuclear track detector, *Radiation Measurements*, 41, 17-22.